Article

Crystal Growth, Thermal and Spectral Properties of Er: LGGG Crystal

Qiaoyun Chi [ID], Lei Liu, Xianhui Xin, Xiuwei Fu *, Zhitai Jia *[ID] and Xutang Tao

State Key Laboratory of Crystal Materials, Shandong University, Jinan 250100, China; 202012830@mail.sdu.edu.cn (Q.C.); 201912614@mail.sdu.edu.cn (L.L.); 202012902@mail.sdu.edu.cn (X.X.); txt@sdu.edu.cn (X.T.)
* Correspondence: fxw@sdu.edu.cn (X.F.); z.jia@sdu.edu.cn (Z.J.)

Abstract: A high-quality Er^{3+}-doped $(Gd_{1-x}Lu_x)_3Ga_5O_{12}$ (Er: LGGG) laser crystal with a size of $\Phi\ 36 \times 45\ mm^3$ was successfully grown by the Czochralski (Cz) method for the first time. The effective segregation coefficient of Er^{3+} was determined to be 0.97, close to 1, and, thus, the uniform high-quality Er: LGGG crystal can be grown. In addition, the thermal and spectroscopic properties of Er: LGGG were investigated. Based on the measured characteristics, the Er: LGGG crystal has a huge potential for use in the 3.0 μm mid-infrared laser because of its outstanding optical quality, extraordinary thermal conductivity and stable structure.

Keywords: mid-infrared laser; Er: LGGG; Czochralski method

1. Introduction

In the past decades, mid-infrared (MIR) lasers have been a hot topic in fields such as biomedicine, spectral detection and space military [1–4]. Currently, one of the main approaches for MIR laser output is the rare-earth lasers, for instance, based on Tm^{3+}, Pr^{3+}, Dy^{3+}, Er^{3+} and Ho^{3+}. Among them, Er^{3+}-doped crystals show promise in producing commercial 2.7~3.0 μm lasers because they can be efficiently pumped by laser diodes (LDs) with wavelengths of 795 or 975 nm. In addition, the Er^{3+}-lasers are likely to own advantages of high power due to the large emission cross section. As is known to all, the 3.0 μm MIR laser can also be applied as a pump sources for obtaining far-infrared tunable lasers from optical parametric oscillator systems [5,6]. Therefore, developing high-quality 3.0 μm MIR Er^{3+}-laser crystals is of great significance.

Up to now, there are many reported Er^{3+}-doped matrix crystals with the spectral range of around 3.0 μm, such as Y_2O_3 [7], Lu_2O_3 [8], $Y_3Al_5O_{12}$ (YAG) [9], $Gd_3Ga_5O_{12}$ (GGG) [10], $Lu_3Ga_5O_{12}$ (LuGG) [11], $Y_3Sc_2Ga_3O_{12}$ (YSGG) [12], and CaF_2 [13]. Among them, the garnet-type Er: GGG crystal is considered as a possible solid-state laser medium because of the advantages of excellent thermal conductivity, excellent physicochemical properties in combination with easy fabrication of large size crystal [14,15]. Er: GGG crystallizes in cubic structure with space group *Ia3d*. Both Er^{3+} and Gd^{3+} occupy the dodecahedral coordinated lattice site. As the radius of Gd^{3+} (1.053 Å) is greater than that of Er^{3+} (1.004 Å), the as-grown crystal showed a non-uniform chemical composition distribution due to the segregation effect, which is very harmful to laser operations. One possible approach to overcome this problem is to engineer the site of crystal structure to match the Er^{3+} size. The Lu^{3+} (0.977 Å) has a smaller radius than Er^{3+}, so that the modified $[Lu_xGd_{1-x}]$ dodecahedral site could be suitable for Er-doping. Accordingly, Lu^{3+} have the advantages of optimizing crystal structure and reducing lattice distortion. However, as far as we know, no Er: $(Lu_xGd_{1-x})_3Ga_5O_{12}$ (Er: LGGG) co-doped crystals have been reported.

The growth of Er: LGGG crystals using the Cz method had not been successfully documented before this work. In the present study, the doping concentrations of Er^{3+} and Lu^{3+} were identified by X-ray fluorescence (XRF). The thermal and optical properties

were essential factors in evaluating the feasibility of experiments and were therefore systematically investigated.

2. Experimental

2.1. Crystal Growth

The Er: LGGG polycrystalline materials with doping levels of 5% Er and 10% Lu were synthesized by the normal solid-state reaction. The source materials in this process were 4N Er_2O_3, Lu_2O_3, Gd_2O_3 and Ga_2O_3 powders (Haipuri Rare Earth Materials Company, Changchun, China). These source materials were weighed stoichiometrically. A 2 wt.% excess of Ga_2O_3 was added due to decomposition and volatilization when the experiment was carried out. After the powders were mixed evenly, the powders were pressed into several columns and sintered in air at 1350 °C for 40 h.

The Cz method was used to grow the Er: LGGG crystal. The synthesized polycrystalline materials were transferred to an Ir crucible (Φ 60 × 60 mm^3). After all raw materials were melted, a single crystal was pulled with an [111] oriented GGG seed under a rotation rate of 10–15 rpm and a pulling rate of 0.79 mm/h. Argon atmosphere was applied during growth to prevent the oxidation of Ir crucible. When the crystal was taken out, it needed to be annealed at 1500 °C for 15 h in the air.

2.2. Characterization Techniques

The successfully grown crystal was processed into crystal samples for characterizations. Single crystal powders were placed in BrukerAXS D2 ADVANCE X-ray diffractometer fitted out Cu-Kα radiation for measuring X-ray diffraction (XRD). Laue back-reflection was performed on Back-Reflection Laue apparatus (Multiwire MWL 120 with North star software) to further make an assessment of the crystalline quality. A square sample of 4 × 4 × 1 mm^3 with the thickness in [111] direction was used for measurement. The concentrations of Er^{3+} and Lu^{3+} were analyzed using the XRF technique (Rigaku, ZSX primus II, Tokyo, Japan).

The thermal expansion was characterized using a Mettler–Toledo thermal-mechanical analyzer (TMA/SDTA840). The sample dimensions were 4 × 4 × 4 mm^3 and the (111) end-faces were fine polished. Specific heat was analyzed using a differential scanning calorimetry (DSC) 8000 differential scanning calorimeter. The grown crystal was processed into 4 × 4 × 1 mm^3 for the test. A same size sample was gilded and measured in a Netzsch Nanoflash model LFA 457 apparatus for thermal diffusivity. The crystal density was measured by the Archimedes method in distilled water at 25 °C. On the basis of the data of specific heat, thermal diffusivity as well as crystal density, the thermal conductivity data were analyzed.

The absorption spectrum was measured by a Cary 7000 equipment. The absorption cross section was calculated on the basis of the measured absorption spectrum data. The fluorescence spectrum measurements were measured using a Hitachi F4500 spectrophotometer. The fluorescence attenuation curve was measured by single photon counting method, and the fluorescence lifetime was fitted according to the fluorescence attenuation curve. All spectral characteristics were evaluated for the polished (111) plates sized 4 × 4 × 1 mm^3.

3. Results and Discussion

3.1. Crystal Growth

The Cz method was used to grow high-quality Er: LGGG crystal with maximum dimensions of Φ 36 × 45 mm^3, as shown in Figure 1. The crystal was free of cracks and inclusions. After polishing, the crystal has high transparency and pale pink color, as shown in Figure 2a. The crystal surface is covered with erosion streaks due to the re-melting during the growth process [16].
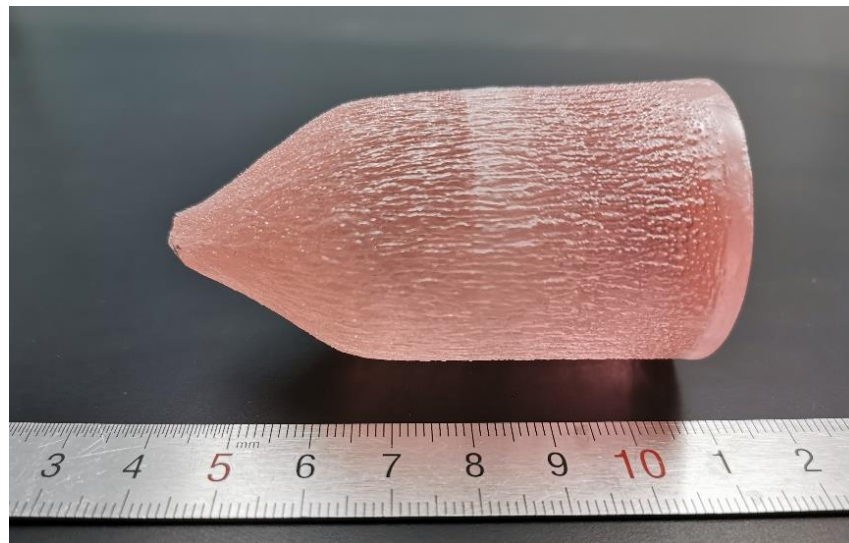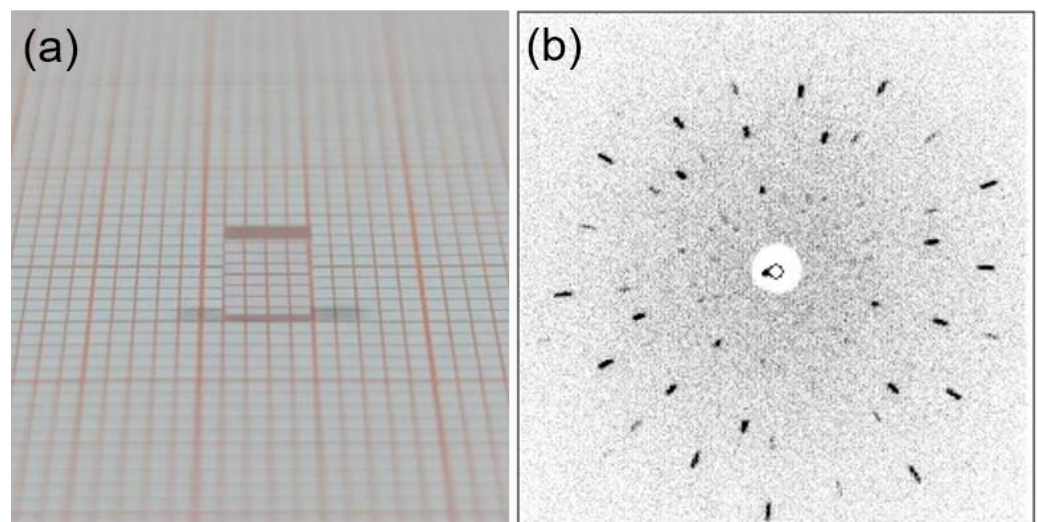
Figure 1. Photograph of as-grown Er: LGGG crystal.

Figure 2. (**a**) The sample ($4 \times 4 \times 4$ mm^3) with a fine (111) end-face polishing used in Laue back-reflection measurements; (**b**) characteristic Laue back-reflection patterns.

3.2. Structural Properties

The XRD pattern of Er: LGGG crystal is displayed in Figure 3. As can be seen, it matches well with the GGG pattern [4] (JCPDS 13-493) simulated from crystal structure, indicating that the single phase was obtained. On the basis of XRD data, the lattice parameters were calculated as $a = b = c = 12.369 \pm 0.002$ Å by software FullProf. The value is smaller than of GGG (12.376 Å) [17] because of smaller radius of the Er^{3+} and Lu^{3+} in reference to that of Gd^{3+}.

The structural quality of Er: LGGG crystal was characterized by the Laue back-reflection measurements. It is obviously seen from Figure 2b that the diffraction spots are clear and bright, and have good symmetry, which shows a high crystalline quality.
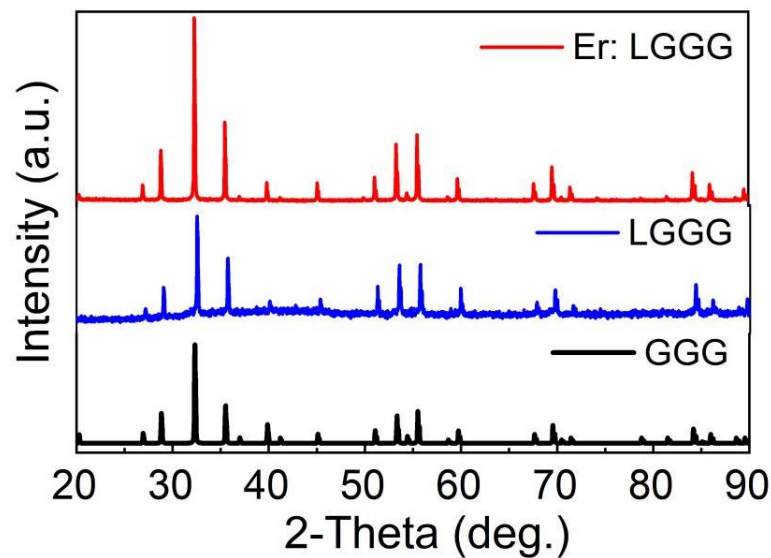
Figure 3. Powder XRD patterns of Er: LGGG and simulated GGG crystals.

3.3. Effective Segregation Coefficient

The effective segregation coefficient of crystal can be calculated on the basis of the formula [18]:

$$k_{eff} = C_s/C_l \tag{1}$$

where C_S and C_l are the ion doping concentrations in the crystal and in raw materials, respectively. Based on the XRF data, the effective segregation coefficients of Er^{3+} and Lu^{3+} in Er: LGGG crystals were calculated to be 0.97 and 1.38, respectively. The effective segregation coefficient of Er^{3+} is approximately equal to 1, which is necessary for rapid and high-quality crystal growth. In contrast, the reported value of Er^{3+} in 10 at.% Er: GGG is as high as 1.56, far from idea value of 1 [19]. Therefore, the lattice engineering for Er: LGGG in this work is very successful.
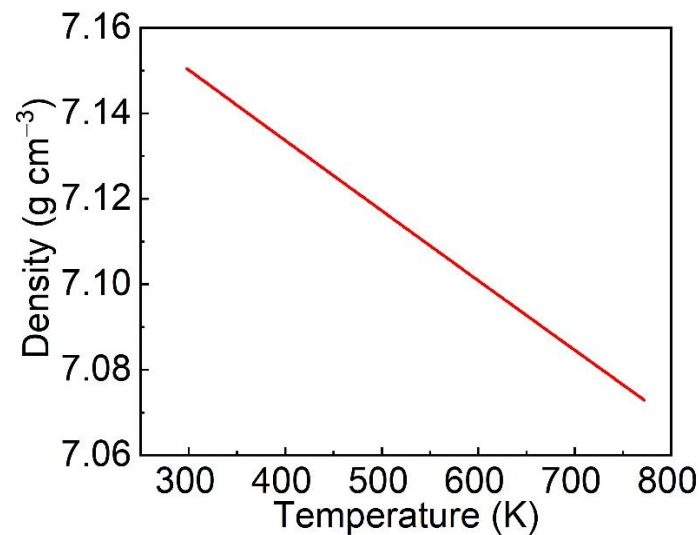
3.4. Crystal Density

Three samples were taken from different parts of the crystal and the density was measured by buoyancy method as shown in Table 1 (m_0 is the sample weight in air, m_1 is the sample weight in deionized water, ρ_{water} is the density of the deionized water at room temperature, ρ_{exp} is the density of the sample, and ρ_{av} is the average density of the sample). The average density of Er: LGGG crystal measured is 7.15 ± 0.02 g cm^{-3} at room temperature, larger than 7.088 g cm^{-3} [20] of GGG crystal due to the more heavy atomic masses of Er^{3+} and Lu^{3+}. Then, the density value of the crystal at different temperatures can be obtained by the following equation [21]:

$$\rho_{\mathrm{T}} = \frac{MZ}{V_T N_A} = \frac{\rho_{T_0}}{1 + 3\alpha \times (T - T_0)} \tag{2}$$

where ρ_T is the crystal density at T, M is the molar weight of the crystal, Z is the number of molecules in the unit cell, V_T is the unit cell volumes at T, ρ_{T_0} is the density at room temperature of 300 K, and α is the thermal expansion coefficients. The average linear expansion coefficient calculated in this work was $\alpha = 7.7096 \times 10^{-6}$ K^{-1}. The density change of Er: LGGG crystal in the temperature range of 298~773 K is shown in Figure 4. With temperature increasing, the density decreases linearly from 7.15 g cm^{-3} at 298 K to 7.07 g cm^{-3} at 773 K.

Table 1. Density of Er-LGGG crystal.

	Sample 1	Sample 2	Sample 3
m_0 (g)	1.0935	2.4696	3.8052
$m_0 - m_1$ (g)	0.1528	0.3435	0.5324
ρ_{water} (g/cm^3)		0.998	
ρ_{exp} (g/cm^3)	7.1437	7.1768	7.1331
ρ_{av} (g/cm^3)		7.15 ± 0.02	

Figure 4. Density of Er: LGGG crystal versus temperature.

3.5. Thermal Properties

Thermal expansion coefficient is a vital physical property of crystal. According to the Neumann principle [22], the thermal expansion coefficients $[\alpha_{ij}]$ are defined by symmetrical second-rank tensor, and $\alpha_{11} = \alpha_{22} = \alpha_{33}$ for Er: LGGG because its structure symmetry is related to cubic system. The temperature-dependent thermal expansion curve of Er: LGGG crystal is presented in Figure 5. The average thermal expansion coefficient was fitted to be 7.71×10^{-6} K^{-1}, comparable with 9.03×10^{-6} K^{-1} of GGG crystal [23].
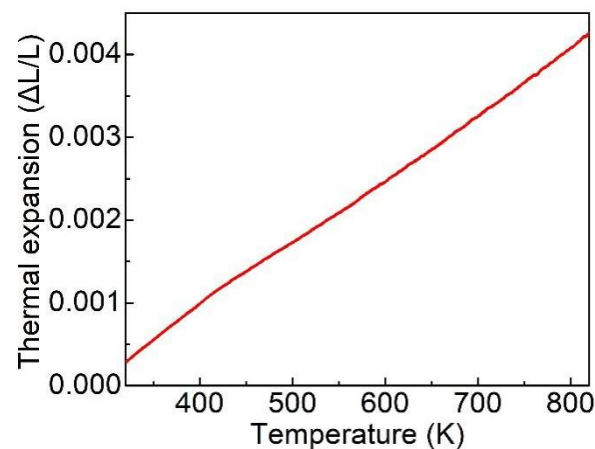
Figure 5. Thermal expansion ratio of Er: LGGG versus temperature.

For laser crystal, the specific heat plays a vital part in affecting the optical damage threshold. Generally speaking, the higher specific heat leads to higher laser damage threshold. The scaling relationship between specific heat and temperature is shown in Figure 6. The specific heat of Er: LGGG crystal increases significantly with temperature

from 0.36 J g^{-1} K^{-1} at 293 K to 0.47 J g^{-1} K^{-1} at 573 K, which is slightly lower than that of GGG crystal [20,24], making Er: LGGG crystal perform better at strong pumping.
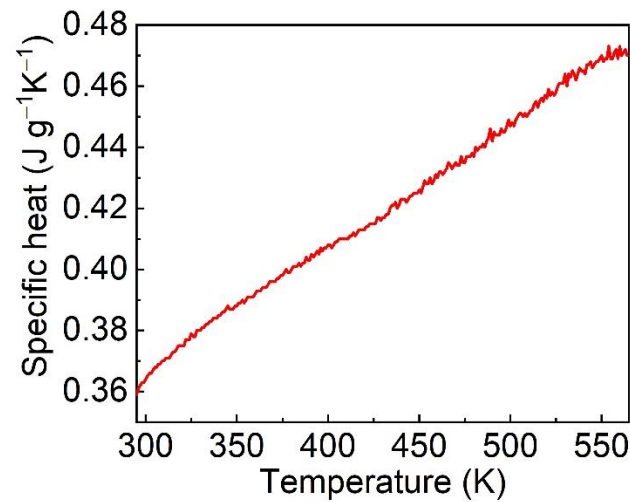

Figure 6. Specific heat of Er: LGGG crystal versus temperature.

The thermal diffusivity is a symmetric second-rank tensor. For the cubic system, there is only one independent principal component. Figure 7a shows the thermal diffusivity of Er: LGGG crystal in terms of temperature. It drops from 2.12 mm^2 s^{-1} at 293 K to 0.81 mm^2 s^{-1} at 773 K. Then, the formula for deriving the thermal conductivity κ can be expressed as follows [25]:

$$\kappa = \lambda \cdot \rho \cdot C_p \tag{3}$$

where λ, ρ and C_p are the thermal diffusivity, density and specific heat of the crystal, respectively, at the corresponding temperature. According to Equation (3), the change of thermal conductivity from 5.43 W m^{-1} k^{-1} at 293 K to 3.28 W m^{-1} k^{-1} at 773 K is shown in Figure 7b, slightly lower than 7.05 W m^{-1} k^{-1} of GGG crystal at room temperature [20].
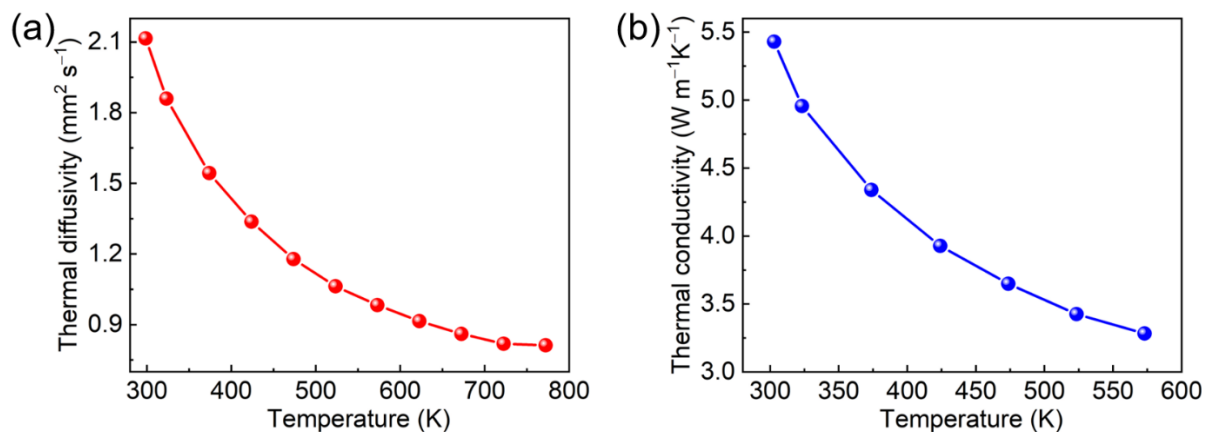

Figure 7. (**a**) Thermal diffusivity and (**b**) calculated thermal conductivity of Er: LGGG crystal in terms of temperature.

3.6. Spectral Properties

The absorption cross section of Er: LGGG crystals within the limits of 350–1800 nm is shown in Figure 8. Seven strong-absorption bands of Er^{3+} centered at 381, 524, 654, 790, 966, 1471 (1532) nm were observed, and they can be attributed to the transition from the ground

state $^4I_{15/2}$ to $^4G_{9/2}$, $^5S_{3/2}$, $^4F_{9/2}$, $^4I_{9/2}$, $^4I_{11/2}$ and $^4I_{13/2}$. The absorption cross section σ can be expressed as follows [19]:

$$\sigma = \frac{\alpha}{N_C} = \frac{A}{N_C L \times \lg e} \tag{4}$$

where α is the absorption coefficient, N_c is the concentration of doping ions, A is the absorbance and L is the thickness of the polished crystal. The maximum absorption cross section of Er: LGGG at the peak of 967 nm is 5.28×10^{-21} cm^2, and its full width at half maximum (FWHM) is about 11 nm. The 967 nm band overlaps well with the commercially available high-power InGaAs LDs. The absorption cross-sectional area of Er: YSGG crystal is 1.56×10^{-21} cm^2 [26], 3.4 times lower than that of Er: LGGG crystal. Therefore, the large absorption bandwidth of Er: LGGG crystal is suitable for pumping and can reduce the temperature dependence for the LDs.
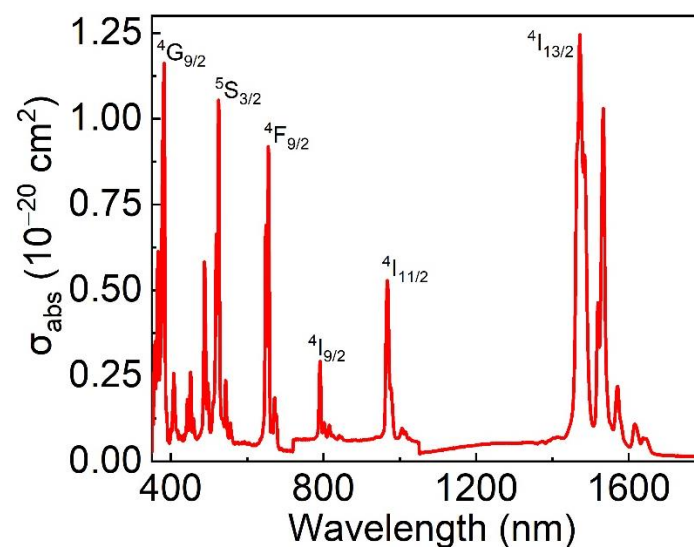

Figure 8. Absorption spectra of the Er: LGGG at room temperature.

Figure 9 is the MIR emission spectrum recorded under the excitation at 967 nm. Two strong fluorescence peaks near 2650 and 2820 nm were observed. The FWHM of MIR emission spectrum are more than 100 nm, indicating the potential to realize tunable and short pulse laser. Furthermore, there is an obvious sub-level jump from $^4I_{11/2}$ to $^4I_{13/2}$ in Er^{3+}. These phenomena fully demonstrated that Er: LGGG crystal shows a promise for the use in the laser field.

Under the excitation of 970 nm pulsed laser, the fluorescence decay curve of Er: LGGG for the upper ($^4I_{11/2}$) laser level was characterized at 2650 nm. In the case of 10 at.% Er: GGG crystal, the fluorescence decay curve fits a single exponential [19]. However, the doping of Lu^{3+} makes the fluorescence decay curve double exponential, as seen in Figure 10. The fitting values are $\tau_1 = 0.063$ and $\tau_2 = 0.805$. Then, through the formula the fluorescence lifetime τ can be expressed as follows:

$$\tau = \frac{A_1 \tau_1^2 + A_2 \tau_2^2}{A_1 \tau_1 + A_2 \tau_2} \tag{5}$$

where A_1 is 0.813, τ_1 is 0.063, A_2 is 0.150, τ_2 is 0.805. The fluorescence lifetime was evaluated to be 0.584 ms ($^4I_{11/2}$).The high concentration of Er^{3+} takes a leading part in the delay of fluorescence intensity. They can realize the rapid pumping of the number of particles in the lower level and recycle the energy by the complex up-conversion and cross-relaxation processes between adjacent ions. The growth of Er-doped crystals with high concentration needs further development.
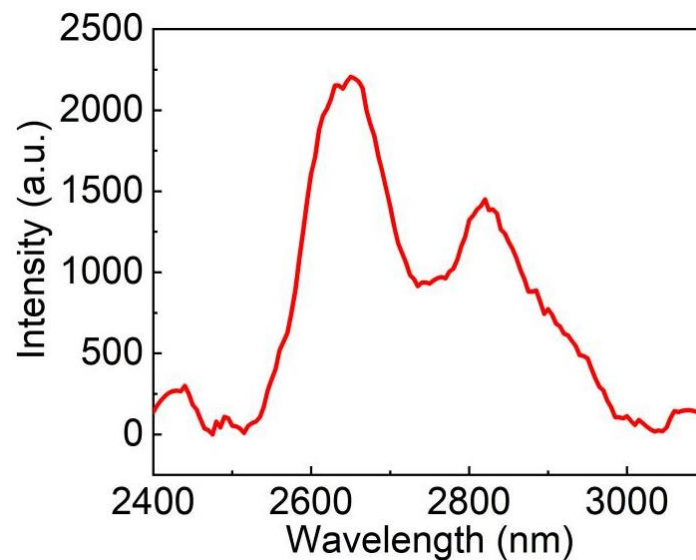
Figure 9. The room-temperature fluorescence spectrum of Er: LGGG under the 967 nm diode excitation.
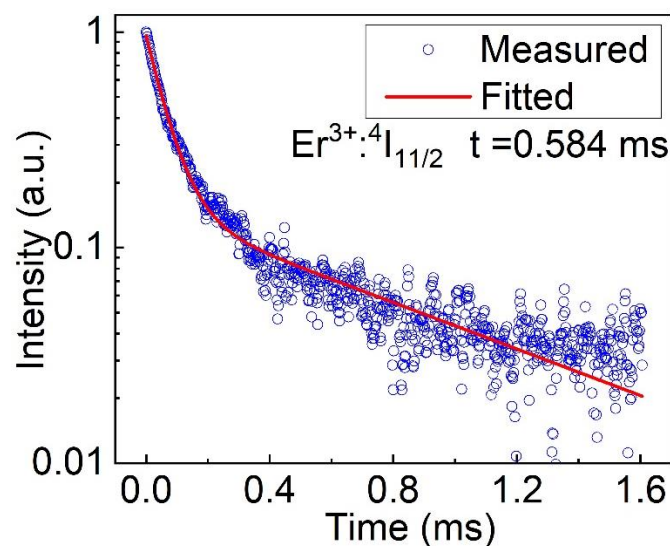

Figure 10. The fluorescence decay curve of Er: LGGG versus time at 2650 nm.

4. Conclusions

In summary, the bulk Er: LGGG crystal with superior quality was successfully grown using the Cz method. The dimension was $\Phi\ 36 \times 45\ \text{mm}^3$. According to the XRF measurements, the effective segregation coefficient of Er^{3+} was 0.97, close to the 1. The thermal and spectral properties were evaluated and analyzed. The coefficient of thermal expansion increases linearly with temperature, and the average linear thermal expansion coefficient was $7.71 \times 10^{-6}\ \text{K}^{-1}$. The specific heat also increased from 0.36 J g^{-1} K^{-1} at 293 K to 0.47 J g^{-1} K^{-1} at 573 K. The thermal diffusivity decreased from 2.12 mm^2 s^{-1} at 293 K to 0.81 mm^2 s^{-1} at 773 K. The thermal conductivity was deduced from 5.43 W m^{-1} k^{-1} at 293 K to 3.28 W m^{-1} k^{-1} at 573 K. In addition, absorption spectrum, fluorescence spectrum and fluorescence decay curve of Er: LGGG were measured at room temperature. The fluorescence lifetime was as high as 0.584 ms ($^4I_{11/2}$) by fitting with the use of single exponential function. The above experimental results proof that the Er: LGGG crystal is a MIR laser material with great potential for applications.

References

1. Skorczakowski, M.; Swiderski, J.; Pichola, W.; Nyga, P.; Zajac, A.; Maciejewska, M.; Galecki, L.; Kasprzak, J.; Gross, S.; Heinrich, A.; et al. Mid-infrared Q-switched Er:YAG laser for medical applications. *Laser Phys. Lett.* **2010**, *7*, 498–504. [CrossRef]
2. Zajac, A.; Skorczakowski, M.; Swiderski, J.; Nyga, P. Electrooptically Q-switched mid-infrared Er:YAG laser for medical applications. *Opt. Lett.* **2004**, *12*, 5125–5130. [CrossRef] [PubMed]
3. Boulon, G. Fifty years of advances in solid-state laser materials. *Adv. Opt. Mater.* **2012**, *34*, 499–512. [CrossRef]
4. Jia, Z.; Tao, X.; Dong, C.; Cheng, X.; Zhang, W.; Xu, F.; Jiang, M. Study on crystal growth of large size Nd^{3+}:$Gd_3Ga_5O_{12}$ (Nd^{3+}:GGG) by Czochralski method. *J. Cryst. Growth* **2006**, *292*, 386–390. [CrossRef]
5. Vodopyanov, K.L.; Ganikhanov, F.; Maffetone, J.P.; Zwieback, I.; Ruderman, W. $ZnGeP_2$ optical parametric oscillator with 3.8–12.4 μm tunability. *Opt. Lett.* **2000**, *25*, 841–843. [CrossRef]
6. Serafetinides, A.A.; Papayannis, A.D.; Fabrikesi, E.T.; Rickwood, K.R.; Wang, Y.; Shi, Y.W.; Miyagi, M.; Croitoru, N.; Harrington, J.; Nubling, R. Lasers, waveguides and fibers for 3.0 μm medical applications. In Proceedings of the Second GR-I International Conference on New Laser Technologies and Applications, Olympia, Greece, 14 July 1998; Volume 3423, pp. 435–440.
7. Wang, L.; Huang, H.T.; Ren, X.J.; Wang, J.; Shen, D.Y.; Zhao, Y.G.; Zhou, W.; Liu, P.; Tang, D.Y. Nanosecond Pulse Generation at 2.7 μm From a Passively Q-Switched $Er:Y_2O_3$ Ceramic Laser. *IEEE J. Sel. Top. Quant. Electron.* **2018**, *24*, 1600906. [CrossRef]
8. Uehara, H.; Tokita, S.; Kawanaka, J.; Konishi, D.; Murakami, M.; Yasuhara, R. A passively Q-switched compact $Er:Lu_2O_3$ ceramics laser at 2.8 μm with a graphene saturable absorber. *Appl. Phys. Express* **2019**, *12*, 022002. [CrossRef]
9. Ziolek, C.; Ernst, H.; Will, G.F.; Lubatschowski, H.; Welling, H.; Ertmer, W. High-repetition-rate, high-average-power, diode-pumped 2.94 μm Er:YAG laser. *Opt. Lett.* **2001**, *26*, 599–601. [CrossRef]
10. You, Z.; Wang, Y.; Xu, J.; Zhu, Z.; Li, J.; Wang, H.; Tu, C. Single-longitudinal-mode Er:GGG microchip laser operating at 2.7 μm. *Opt. Lett.* **2015**, *40*, 3845–3849. [CrossRef]
11. You, Z.Y.; Li, J.F.; Wang, Y.; Chen, H.B.; Zhu, Z.J.; Tu, C.Y. Spectroscopic and laser properties of Er:LuGG crystal at 2.8 μm. *Appl. Phys. Express* **2019**, *12*, 052019. [CrossRef]
12. Nie, H.K.; Hu, Q.Q.; Zhang, B.T.; Sun, X.L.; Tian, H.L.; Wang, Y.R.; Yan, B.Z.; Jia, Z.T.; Yang, K.J.; Tao, X.T.; et al. Highly Efficient Continuous-Wave and Passively Q-Switching 2.8 μm Er:YSGG Laser. *IEEE Photon. Technol. Lett.* **2018**, *30*, 1400–1403. [CrossRef]
13. Li, C.; Liu, J.; Guo, Z.N.; Zhang, H.; Ma, W.W.; Wang, J.Y.; Xu, X.D.; Su, L.B. Black phosphorus saturable absorber for a diode-pumped passively Q-switched $Er:CaF_2$ mid-infrared laser. *Opt. Commun.* **2018**, *406*, 158–162. [CrossRef]
14. Smirnov, V.A.; Shcherbakov, I.A. Rare-earth scandium chromium garnets as active media for solid-state lasers. *IEEE J. Quant. Electron.* **1988**, *24*, 949–959. [CrossRef]
15. Pollack, S.A.; Chang, D.B.; Birnbaum, M.; Kokta, M. Upconversion-pumped 2.8–2.9 μm lasing of Er^{3+} ion in garnets. *J. Appl. Phys.* **1991**, *70*, 7227–7239. [CrossRef]
16. Ding, Y.C.; Zhao, G.J.; Xu, X.D. Crystal growth and spectroscopic properties of erbium doped Lu_2SiO_5. *J. Cryst.* **2010**, *312*, 2103–2106. [CrossRef]
17. Brandle, C.D. Growth of 3″ diameter $Gd_3Ga_5O_{12}$ crystals. *J. Appl. Phys.* **1978**, *49*, 1855–1858. [CrossRef]
18. Jia, Z.T.; Tao, X.T.; Yu, H.H.; Dong, C.M.; Zhang, J.; Zhang, H.J.; Wang, Z.P.; Jiang, M.H. Growth and properties of $Nd:(Lu_xGd_{1-x})_3Ga_5O_{12}$ laser crystal by Czochralski method. *Opt. Mater.* **2008**, *31*, 346–349. [CrossRef]
19. Wang, Y.; You, Z.Y.; Li, J.F.; Zhu, Z.J.; Ma, E.; Tu, C.Y. Spectroscopic investigations of highly doped $Er^{3+}:GGG$ and $Er^{3+}/Pr^{3+}:GGG$ crystals. *J. Phys. D* **2009**, *42*, 215406. [CrossRef]
20. Krupke, W.F.; Shinn, M.D.; Marion, J.E.; Caird, J.A.; Stokowski, S.E. Spectroscopic, optical, and thermomechanical properties of neodymium-doped and chromium-doped gadolinium scandium gallium garnet. *J. Opt. Soc. Am.* **1986**, *3*, 102–114. [CrossRef]
21. Zhang, J.J.; Zhang, Z.H.; Sun, Y.X.; Zhang, C.Q.; Tao, X.T. Anisotropic thermal properties of the polar crystal $Cs_2TeMo_3O_{12}$. *J Solid State Chem.* **2012**, *195*, 120–124. [CrossRef]
22. Shi, Z.B.; Zhang, H.J.; Wang, J.Y.; Yu, Y.G.; Wang, Z.P.; Yu, H.H.; Sun, S.Q.; Xia, H.R.; Jiang, M.H. Growth and characterization of Nd:CLNGG crystal. *J. Cryst. Growth* **2009**, *311*, 3792–3796. [CrossRef]

23. Tao, D.J.; Zhu, G.X.; Yan, R.S.; Liu, F.Y.; Guo, X.A.; Yin, S.T. Czochralski Growth of Gadolinium Gallium Garnet (GGG) Single Crystals. *IEEE J. Quantu. Electron.* **2003**, *20*, 550–552.

24. Ahn, J. Thermal and optical properties of gadolinium gallium garnet. *Mater. Res. Bull.* **1982**, *17*, 1393–1399. [CrossRef]

25. Fu, X.W.; Jia, Z.T.; Li, Y.B.; Yuan, D.S.; Dong, C.M.; Tao, X.T. Growth and characterization of Nd:LGGG laser crystal. *J. Cryst.* **2012**, *353*, 72–76. [CrossRef]

26. Wang, Y.; Li, J.; Zhu, Z.; You, Z.; Xu, J.; Tu, C. Dual function of Nd^{3+} in Nd, Er:LuYSGG crystal for LD pumped 3.0 μm mid-infrared laser. *Opt. Express* **2015**, *23*, 18554–18562. [CrossRef] [PubMed]